A Wideband Beam-Scanning Reflectarray Based on the 1-bit Tightly Coupled Unit Cell

Wenting Li, *Member, IEEE*, Zhikang Ai, Yejun He, *Senior Member, IEEE*, Chong Zhang, *Member, IEEE*, Yao Gao, Ruiyang Li, and Steven Gao, *Fellow, IEEE*

***Abstract*— In this article, a wideband beam-scanning reflectarray antenna is proposed. The reflecting surface is built based on the 1-bit tightly coupled elements. The phase control is achieved by loading radio frequency (RF) switches on the delay lines of the elements. To obtain better sidelobe levels (SLLs) and beam directions, the state of the RF switch on the reflecting surface is optimized by applying particle swarm optimization (PSO). Additionally, a novel method for calculating the reflection phase of the strongly coupled elements is proposed. To verify the design, a prototype reflectarray consisting of 27 × 9 elements is simulated, fabricated, and measured. Measured results show that the proposed reflectarray can achieve ±45° beam scanning from 4 to 6 GHz with the stable main beam.**

***Index Terms*— Beam-scanning, strongly coupled elements, wideband reflectarray.**

I. Introduction

BEAM-SCANNING reflectarray has received extensive interest from many researchers in recent years. Compared with traditional phased-array antennas that use complex beamforming networks, the beam-scanning reflectarray adopts the spatial feed structure, offering the advantages of lower cost and simpler structure [1]. The beam-scanning reflectarray can achieve beam focusing and beam scanning by changing the reflection phase distributions on the reflecting surface. Many researchers have employed methods such as introducing devices like varactor diodes [2], [3], [4] and p-i-n diodes [5], [6], [7], as well as using tunable materials like tunable liquid crystals [8], [9], to achieve dynamic beam scanning. In [10], a novel dual-port dual-beam reconfigurable antenna is presented. By changing the states of the p-i-n diodes on the reconfigurable metal lines, the two ports can independently perform beam scanning.

In [11], [12], and [13], the 1-bit reconfigurable reflectarray based on radiating element rotation is proposed. This approach can achieve the 180° phase difference while maintaining low losses. In [14], [15], [16], and [17], p-i-n diodes are embedded in the delay lines. In this way, the length of the current path on the delay line is controlled, thus achieving the reflection phase change. Specifically, unlike the traditional method of placing p-i-n diodes on the microstrip line, in [17], the p-i-n diodes are inserted into the center of a coupling slot on the ground plane. This method significantly reduces the losses caused by the p-i-n diodes. In [18], a highly integrated reconfigurable electromagnetic (EM) surface is proposed, which integrates p-i-n diodes onto the radiating patch. By changing the state of the p-i-n diode, the operating mode and phase response of the unit are adjusted.

Whether using unit rotation or controlling the length of delay lines to achieve the 1-bit phase difference, these reflectarrays face the challenge of narrow bandwidth. The main reasons for this limitation are the bandwidth constraints of the unit cell and the differential spatial phase delay. Many methods have been introduced to improve the bandwidth of the reflectarray. In [19], a broadband reflectarray based on magneto-electric dipole unit cell is proposed, which eliminates the influence of frequency by resonating the magnetic and electric dipoles at the same frequency. In [20], a wideband reflectarray based on the polarization rotating wideband element is proposed, which achieves the 180° phase shift from 5.4 to 12.7 GHz. In [21] and [22], by introducing the tightly coupled elements, the single-polarized and the dual-polarized tightly coupled wideband reflectarrays are proposed, respectively. The reflection phase is controlled by changing the length of the delay line. By introducing the concept of equivalent distance delay, the influence of frequency on the reflection phase is eliminated. However, these two designs only achieve broadband reflectarrays when the beam direction is fixed.

In this article, a wideband 1-bit tightly coupled beam-scanning reflectarray is proposed. The element of the proposed design is based on the tightly coupled element in [21]. First, to achieve beam scanning, radio frequency (RF) switches are introduced on the delay lines of the reflectarray ele-

Received 5 August 2024; revised 14 February 2025; accepted 8 March 2025. Date of publication 24 March 2025; date of current version 9 July 2025. This work was supported in part by the National Key Research and Development Program of China under Grant 2023YFE0107900, in part by the National Natural Science Foundation of China under Grant 62101341 and Grant 62071306, and in part by Shenzhen Science and Technology Innovation Program under Grant JCYJ20230808105510020. *(Corresponding author: Wenting Li.)*

Wenting Li, Zhikang Ai, and Yejun He are with the State Key Laboratory of Radio Frequency Heterogeneous Integration, School of Electronic and Information Engineering, Shenzhen University, Shenzhen 518000, China (e-mail: w.li@szu.edu.cn).

Chong Zhang is with the School of Information Science and Engineering, Shenyang University of Technology, Shenyang 710000, China.

Yao Gao is with the School of Information Engineering, Chang'an University, Xi'an 710000, China.

Ruiyang Li is with the School of Electrical and Information Engineering, Zhengzhou University, Zhengzhou 450000, China.

Steven Gao is with the Department of Electronic Engineering, Chinese University of Hong Kong, Hong Kong, China.

Digital Object Identifier 10.1109/TAP.2025.3552235

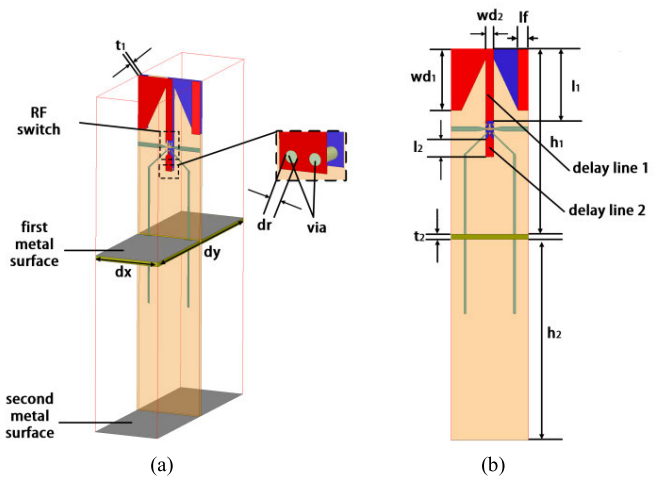

(a) (b)

Fig. 1. (a) Side view and (b) front view of the 1-bit reconfigurable unit cell.

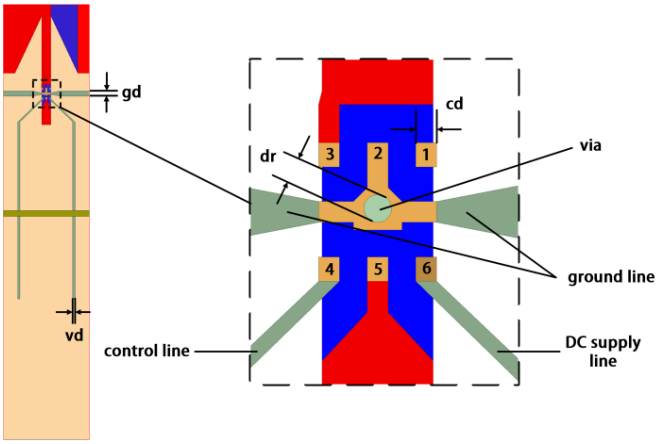

Fig. 2. Solder pad of the RF switch and the dc lines.

ments. The reflection phase of the unit cell can be controlled by RF switches. Since the switches have two states, on and off, the unit cell also has two reflection phases. This method conveniently implements the broadband 1-bit reconfigurable unit cell. Although, in [23], RF switches have been introduced into tightly coupled elements to control the reflection phase, there are some limitations. On the one hand, the impact of dc bias lines is not considered, and only simulation results are given. On the other hand, two RF switches are applied in one element to control the reflection phase [23], while the proposed reflectarray in this article only employs one RF switch in one element. Second, after achieving the 1-bit reconfigurability of the unit cell, it is necessary to determine the switch states on the reflecting surface. This requires mapping the required reflection phase on the reflecting surface to the RF switch state of the unit cell. When applying the traditional geometric optical mapping (GOM), the sidelobe levels (SLLs) of radiation patterns are high. To improve SLLs, particle swarm optimization (PSO) is proposed to optimize the states of the RF switch on the reflecting surface. More importantly, a novel method to calculate the reflection phase of elements with strong coupling is proposed. By applying this method, the radiation patterns at low frequencies are computed more accurately.

This article is organized as follows. Section II discusses the design of the broadband 1-bit beam-scanning reflectarray. Section III presents the design and optimization of the switch states on the reflecting surface. Section IV gives the simulated and measured results of the fabricated prototype. Section V concludes this article.

II. Design of Wideband 1-bit Beam-Scanning Reflectarrays

In this section, the tightly coupled 1-bit unit cell is designed. Based on the proposed unit cell, a wideband beam-scanning reflectarray is built.

A. 1-bit Reconfigurable Tightly Coupled Unit Cells

The structure of the tightly coupled unit cell is shown in Fig. 1. The unit cell includes a tightly coupled dipole, a pair of delay lines with two metalized vias at the ends, an RF switch, and the dc lines. The dipole is printed on the Rogers 4350B. The dimension of the unit cell is $d_x \times d_y$, and the distance from the top of the unit cell to the first metal plane is h_1. d_x, d_y, and h_1 affect the impedance bandwidth of the unit cell significantly.

TABLE I
Parameters of the Unit Cell

Parameter	t_1	t_2	d_x	d_y	wd_1	wd_2	l_f	l_2
Value(mm)	0.508	0.508	23	7.5	6	1.2	1.5	2
Parameter	l_1	gd	vd	cd	dr	h_1	h_2	
Value(mm)	7	0.45	0.2	0.15	0.2	18	20	

To control the reflection phase of the unit cell, the RF switch is introduced. The RF switch is placed on one of the delay lines, which is divided into two parts: delay line 1 and delay line 2. The RF switch is a single-pole double-throw switch (NJG1818K75). The solder pad structure and dc lines of the RF switch in the unit cell are shown in Fig. 2. Pin 1 and pin 3 are two RF ports of the switch, and pin 5 is the RF common port. In the proposed design, pin 3 is connected to delay line 1, and pin 5 is connected to delay line 2. Pin 2 is connected to the ground. Pin 4 is used to input the control signal, and pin 6 is the dc voltage supply input. The parameters of the unit cell are listed in Table I.

The reflection coefficient of the unit cell is shown in Fig. 3. For the unit cell without the RF switch, the reflection coefficient is below -10 dB from 2 to 7 GHz. When the RF switch and dc lines are introduced, the reflection coefficient deteriorates slightly, which remains below -7 dB from 2 to 6 GHz.

The reflection phase difference between the ON-state and OFF-state of the unit cells $\Delta\varphi$ can be written as follows:

$$\Delta\varphi = \varphi_{OFF} - \varphi_{ON} \tag{1}$$

where φ_{OFF} is the reflection phase when the RF switch is off and φ_{ON} is that when the RF switch is on. The unit cell could reflect the EM energy from the feeding antenna. Fig. 4 shows

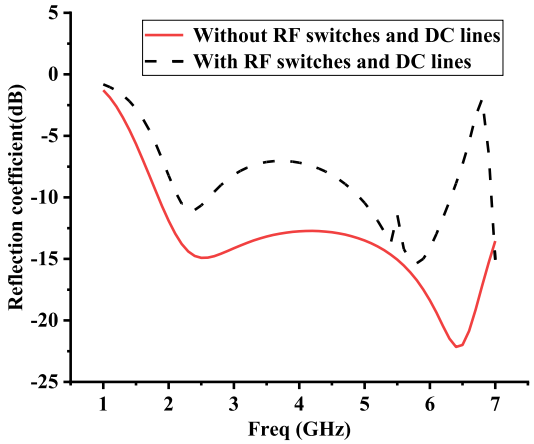

Fig. 3. Reflection coefficient of the unit cell.

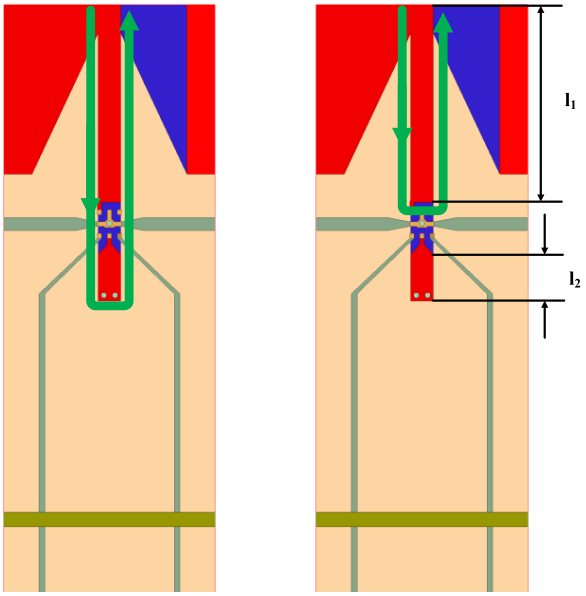

(a) (b)

Fig. 4. Energy flow on the delay line when the RF switch is (a) on and (b) off.

the energy flow on the delay line when the RF switch is on and off. Therefore, $\Delta\varphi$ can also be expressed as follows:

$$\Delta\varphi = \Delta\varphi_1 + \Delta\varphi_2 \tag{2}$$

where $\Delta\varphi_1$ is the phase shift caused by delay line 2, and $\Delta\varphi_2$ is the phase shift caused by the RF switch. $\Delta\varphi_1$ can be expressed as follows:

$$\Delta\varphi_1 = 2 * l_2 * \frac{2\pi f\sqrt{\varepsilon_{re}}}{c} + \pi \tag{3}$$

where f is the frequency. ε_{re} is the relative permittivity. c is the speed of light in the vacuum. $\Delta\varphi_2$ can be expressed as follows:

$$\Delta\varphi_2 = 2 * phase(S_{RF}) \tag{4}$$

where $phase\ (S_{RF})$ is the transmission phase of the RF switch from pin 3 to pin 5. As both $\Delta\varphi_1$ and $\Delta\varphi_2$ are affected by frequency, $\Delta\varphi$ changes with varying frequency. At the same time, the introduction of dc lines also affects the reflection phase of the unit cell. Therefore, to achieve the 1-bit reconfigurable unit cell over a wide frequency range, it is crucial to determine l_1 and l_2.

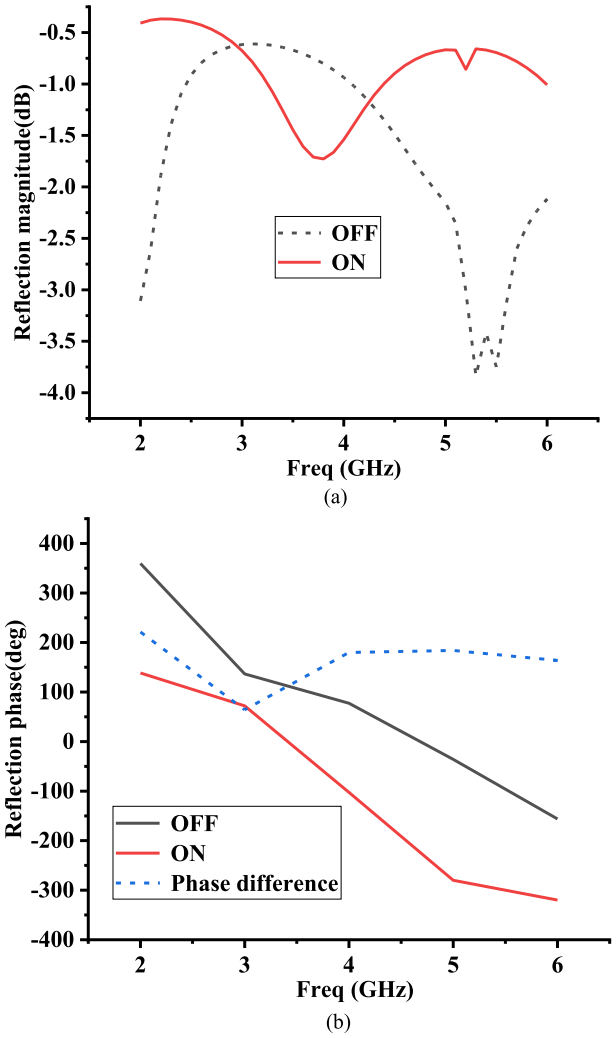

Fig. 5. (a) Amplitude response and (b) phase response of the unit cell.

$\Delta\varphi$ at frequency f_n is $\Delta\varphi(f_n)$. Assume that there are N frequency points in the working band. $D(\varphi)$ is given by

$$D(\varphi) = \sum_{i=1}^{N} |\Delta\varphi(f_i) - 180°|. \tag{5}$$

If $\Delta\varphi$ is 180° for all frequencies, $D(\varphi)$ should be zero. By scanning l_1 and l_2, it is found that when $D(\varphi)$ is minimized, $l_1 = 7$ mm and $l_2 = 1.65$ mm. Fig. 5 shows the amplitude and phase responses of the unit cell. It can be seen that when the RF switch is on, the reflection magnitude of the unit cell is above -2 dB. When the RF switch is off, the reflection magnitude of the unit cell deteriorates at 5.5 GHz, reaching around -3.5 dB. Table II shows φ_{OFF}, φ_{ON}, and $\Delta\varphi$ of the unit cell at different frequencies. It can be seen that at 4, 5, and 6 GHz, $\Delta\varphi(f_n)$ is within 180 $\pm$ 20°.

TABLE II

φ_{OFF}, φ_{ON}, AND $\Delta\varphi$ OF THE UNIT CELL ($l_1 = 7$ mm AND $l_2 = 1.65$ mm)

Freq(GHz)	2	3	4	5	6
φ_{OFF} (deg)	359.61	136.52	77.45	-35.88	-156.07
φ_{ON} (deg)	138.42	72.26	-102.45	-219.96	-319.96
$\Delta\varphi$ (deg)	221.19	64.26	179.9	184.08	163.89

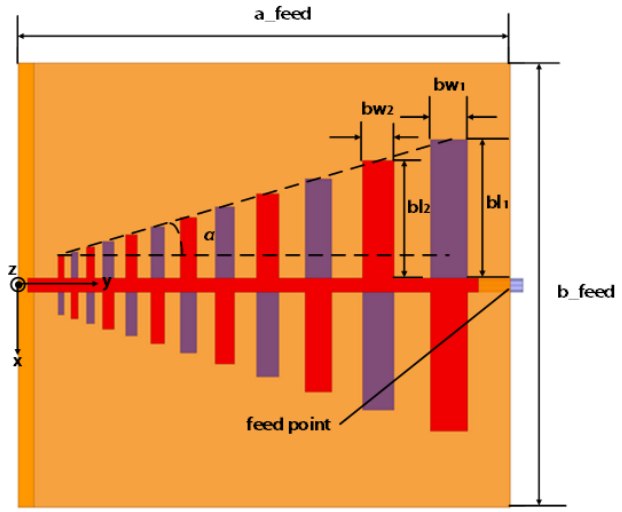

Fig. 6. Structure of the LPDA.

TABLE III

COORDINATES OF THE PHASE CENTER OF LPDA

Freq (GHz)	4	5	6
$p(x,y,z)$	(0,33.74,0)	(0,25.19,0)	(0,19.05,0)

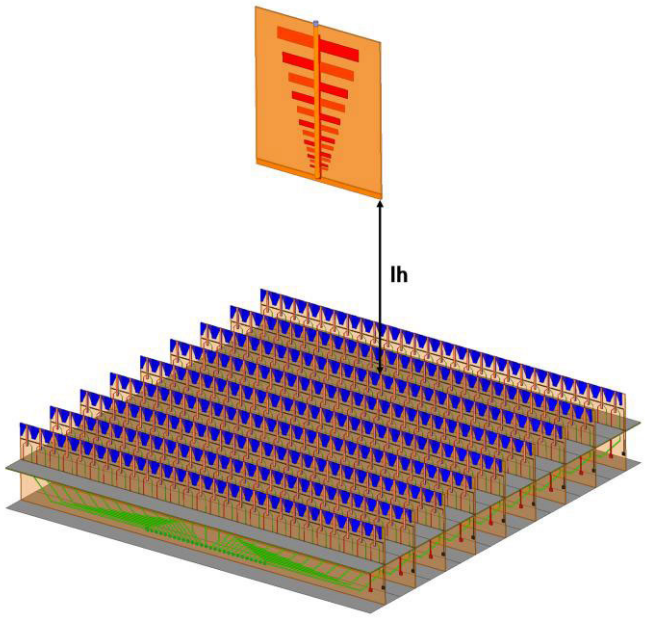

Fig. 7. Structure of the reflectarray.

However, at 2 and 3 GHz, $\Delta\varphi(f_n)$ deviates significantly from 180°. Therefore, 4–6 GHz is chosen as the working band of the unit cell.

B. Feed Antenna

The broadband feed antenna is a log-periodic dipole array (LPDA), which is shown in Fig. 6. The antenna consists of a pair of microstrip and a dipole array. Both the dipoles and the microstrip lines are printed on Rogers 4350B with a thickness of 0.762 mm. The antenna is fed by a coaxial cable. The dimension of the substrate is *a_feed* × *b_feed*. The width of the microstrip is 2.2 mm. The angle $\alpha = 19.22°$. The length bl_1 and width bw_1 of the first dipole are 21.86 and 5.83 mm, respectively. The ratio between the adjacent dipoles satisfies

$$\frac{bl_1}{bl_2} = \frac{bw_1}{bw_2} = 1.18. \tag{6}$$

According to [22], to generate a beam in a specific direction, the required reflection phase of each element on the reflecting surface is related to the distance from the phase center of the feed to the element d_i, which can be written as follows:

$$d_i = \sqrt{(x_i - x_f)^2 + (y_i - y_f)^2 + (z_i - z_f)^2} \tag{7}$$

where (x_i, y_i, z_i) is the coordinate of the unit cell on the reflecting surface and (x_f, y_f, z_f) is the coordinate of the phase center of the feed at frequency f. The phase center of LPDA changes at different frequencies. The phase center of the LPDA $p(x, y, z)$ at each frequency point is shown in Table III.

C. Reflectarray Configuration

To verify the beam scanning capability of the proposed design, a reflectarray consisting of 27 × 9 unit cells is constructed. The structure of the reflectarray is shown in Fig. 7. The dimension of the reflecting surface is 207 × 202.5 × 38 mm^3, and the distance from the feed antenna to the reflecting surface *lh* is 111 mm.

III. DESIGN AND OPTIMIZATION OF THE STATES OF THE RF SWITCH ON THE REFLECTING SURFACE

In this section, RF switch states on the reflecting surface are determined and optimized. A new method is proposed to calculate the reflection phase of strongly coupled elements.

A. RF Switch States Distribution

To generate the main beam with the specific direction, the required reflection phase $\Phi(f_n)$ for each unit cell on the reflecting surface at frequency f_n can be calculated according to [21] and [24]. Then, the states of the RF switch for each unit cell are determined by

$$\text{states} = \begin{cases} OFF, & \Phi(f_n) \in \left[\Delta\varphi(f_n) - \dfrac{\pi}{2}, \Delta\varphi(f_n) + \dfrac{\pi}{2}\right] \\ ON, & \text{else.} \end{cases} \tag{8}$$

This method to calculate the RF switch states is called GOM. Take the beam direction being 30° at 5 GHz for

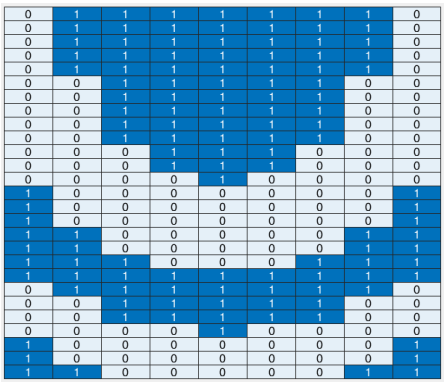

Fig. 8. Distribution of RF switch states when the scan angle is 30°.

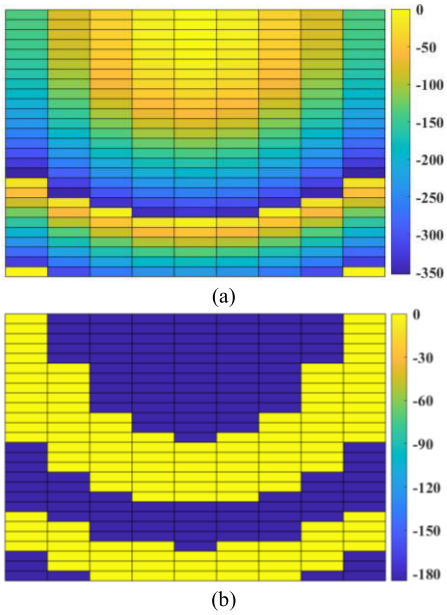

Fig. 9. (a) Ideal reflection phase. (b) Quantized reflection phase.

an example. Fig. 8 shows the RF switch states by GOM on the reflecting surface, where 0 represents the ON-state and 1 represents the OFF-state. Fig. 9 shows the ideal reflection phase and the quantized reflection phase calculated by GOM. It can be seen that the ideal reflection phase is continuously distributed on the reflecting surface, while the reflection phase calculated based on GOM only has two states, which inevitably leads to the deterioration of the radiation pattern.

The radiation patterns of the reflectarray are calculated according to the array antenna theory. The radiation patterns when the beam directions are 0°, 15°, and 30° at 4, 5, and 6 GHz are shown in Fig. 10. It can be observed that the radiation pattern from GOM deteriorates significantly in SLLs compared with those from the ideal reflection phase. Specifically, at 4 GHz, with beam directions being 15° and 30°, the SLLs are only around −8 dB.

B. Particle Swarm Optimization

To obtain better radiation patterns, PSO is introduced. The variables to be optimized are the states of the RF switches on the reflecting surface. The loss function F_{total} includes

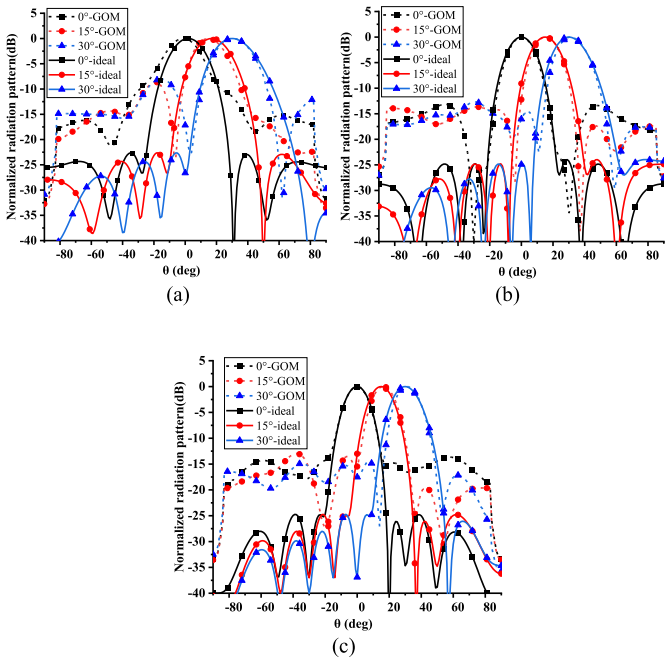

Fig. 10. Calculated radiation patterns at (a) 4, (b) 5, and (c) 6 GHz.

2-D radiation pattern loss function F_{2D} and the 3-D radiation pattern loss function F_{3D}. F_{3D} is used to maintain the basic shape of the 3-D radiation pattern, while F_{2D} is used to optimize the 2-D radiation pattern. F_{total} is expressed as follows:

$$F_{total} = aF_{2D} + bF_{3D} \tag{9}$$

where a and b are normalized weighting coefficients. The 2-D radiation pattern loss function F_{2D} includes the SLL loss function F_{SLL} and beam direction loss function F_{BD}. It is written as follows:

$$F_{2D} = a_1 F_{SLL} + a_2 F_{BD} \tag{10}$$

where a_1 and a_2 are normalized weighting coefficients.

F_{SLL} is defined as follows:

$$F_{SLL} = \begin{cases} 0, & SLL_{cal} < SLL_0 \\ (SLL_{cal} - SLL_0)^2, & SLL_{cal} \geq SLL_0 \end{cases} \tag{11}$$

where SLL_{cal} is the SLL calculated in PSO. SLL_0 is the desired target SLL. When SLL_{cal} is below SLL_0, it meets the requirement, and the loss function is set to 0. Otherwise, the loss function is the square of the difference between SLL_{cal} and SLL_0.

F_{BD} is defined as follows:

$$F_{BD} = \begin{cases} (\theta_{cal} - \theta_{min})^2, & \theta_{cal} < \theta_{min} \\ (\theta_{cal} - \theta_{max})^2, & \theta_{cal} > \theta_{max} \\ 0, & \theta_{min} \leq \theta_{cal} \leq \theta_{max} \end{cases} \tag{12}$$

where θ_{cal} is the beam direction of the 2-D radiation pattern calculated in PSO. θ_{max} and θ_{min} are the upper and lower bounds of the target beam direction, used to constrain the beam direction. When the calculated beam direction is between θ_{min} and θ_{max}, it is considered to meet the requirement, and the

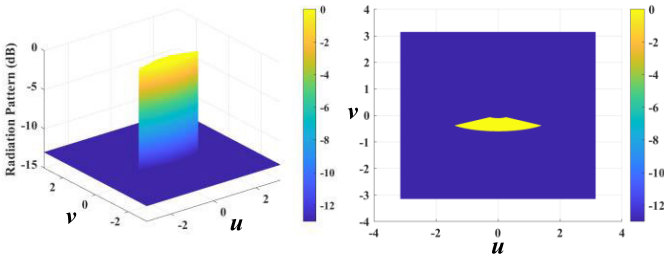

(a) (b)

Fig. 11. Defined mask model. (a) Side view. (b) Top view.

TABLE IV
HYPERPARAMETER VALUES FOR A BEAM DIRECTION OF 30° AT 5 GHz

parameters	a:b	a_1: a_2	SLL_0	θ_{min}	θ_{max}
value	2:1	5:4	-20dB	28°	32°
parameters	θ_l	θ_u	φ_l	φ_u	SLL_{mask}
value	0°	60°	20°	160°	-15dB

loss function is 0. Otherwise, the loss function is the square of the difference between θ_{cal} and θ_{max} or θ_{min}.

The loss function F_{3D} for the 3-D radiation pattern mainly involves the SLL. Before defining F_{3D}, it is necessary to define the mask of the 3-D radiation pattern [25], which is defined as follows:

$$Mask(u,v) = \begin{cases} 0, & (u,v) \in main\ beam \\ SLL_{mask}, & (u,v) \notin main\ beam \end{cases} \tag{13}$$

where SLL_{mask} is the SLL of the mask, which is applied to maintain the basic shape of the 3-D radiation pattern. Therefore, the value of SLL_{mask} can be set slightly higher than SLL_0. u and v are two intermediate variables, which can be expressed as follows:

$$\begin{cases} u = -kd_x sin\theta cos\varphi \\ v = -kd_y sin\theta sin\varphi \end{cases} \tag{14}$$

where k is the propagation constant in free space. The range of the "main beam" is expressed as follows:

$$Main\ beam(\theta,\varphi) = \begin{cases} \theta_l < \theta < \theta_u \\ \varphi_l < \varphi < \varphi_u \end{cases} \tag{15}$$

where θ_l, θ_u, φ_l, and φ_u are hyperparameters used to define the main beam range. The mask is shown in Fig. 11. F_{3D} is defined as follows:

$$F_{3D} = \begin{cases} \sum_u \sum_v (NP(u,v) - SLL_{mask})^2, \\ \qquad NP(u,v) > Mask(u,v) \\ 0, \qquad NP(uv) < Mask(uv) \end{cases} \tag{16}$$

where $NP(u,v)$ is the normalized 3-D radiation pattern. The hyperparameter settings vary for different frequencies and beam directions. The relevant hyperparameter settings for a beam direction of 30° at 5 GHz are shown in Table IV.

After determining the loss functions for both 2-D and 3-D radiation patterns, an iterative procedure is employed to optimize the RF switch states at frequencies of 4, 5, and 6 GHz, respectively, when the beam directions are −30°, −15°, 0°, 15°, and 30°. To reduce the number of iterations, the initial RF switch states are given by GOM.

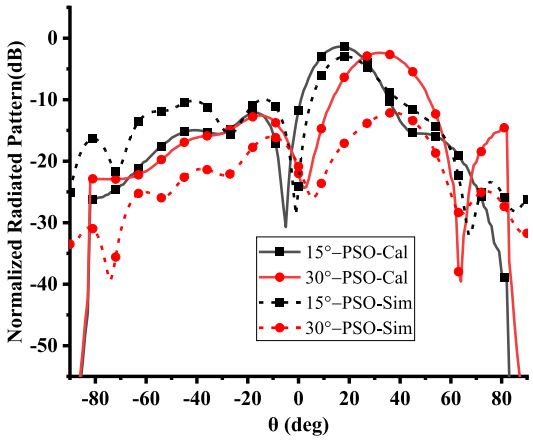

Fig. 12. 2-D radiation patterns from PSO and simulation at 4 GHz.

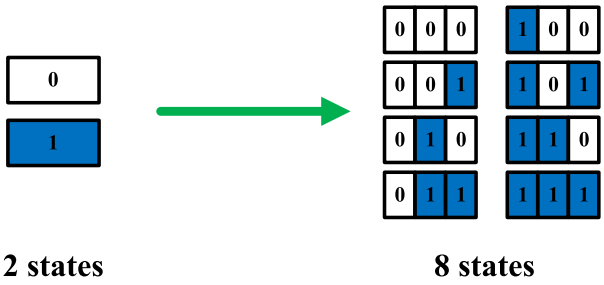

Fig. 13. Change of the strong coupling element states.

TABLE V
SIMULATED REFLECTION PHASES AT 4 GHz

state	000	001	010	011
Phase(deg)	-105.31	109.17	109.13	85.23
state	100	101	110	111
Phase(deg)	109.42	85.33	85.13	77.35

C. Strong Coupling Elements Reflection Phase Calculation

After the radiation patterns are optimized by PSO, the reflectarray is simulated. However, it is found that the simulation radiation patterns at 4 GHz are significantly different from the results calculated by PSO. This difference is particularly noticeable when the scanning angle is large. Fig. 12 presents the calculated and simulated radiation patterns, with beam directions being 15° and 30° at 4 GHz. It can be seen that the SLLs of the simulated radiation patterns are quite different from the calculated results. When the beam direction is 30°, the simulated radiation patterns are totally distorted. At 5 and 6 GHz, the differences between the simulated and calculated radiation patterns are much smaller.

This phenomenon may result from the coupling effect between the elements. As the proposed reflectarray is based on the tightly coupled element, the coupling between adjacent elements is much stronger than that of the conventional reflectarray element. At the same time, the coupling is enhanced as the frequency decreases, because the electronic distance

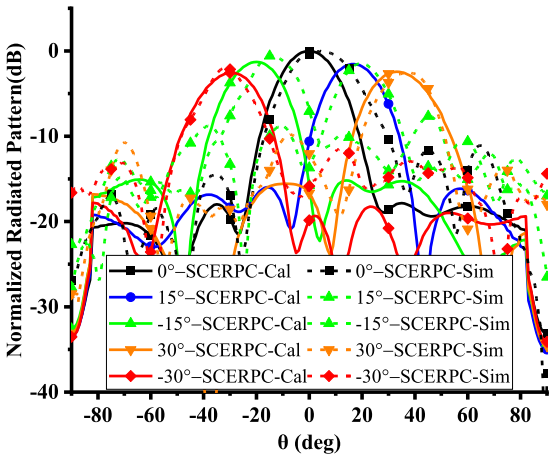

Fig. 14. Simulated and calculated radiation patterns from PSO with SCERPC at 4 GHz.

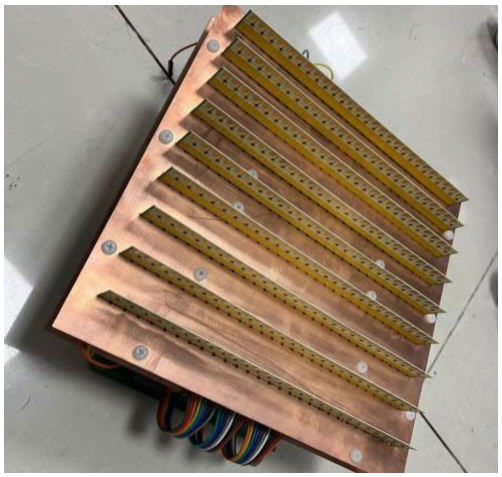

Fig. 15. Prototype of the reconfigurable reflectarray.

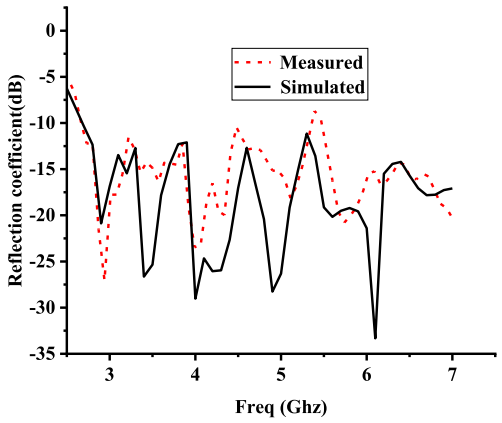

Fig. 16. Reflection coefficient of the feed antenna.

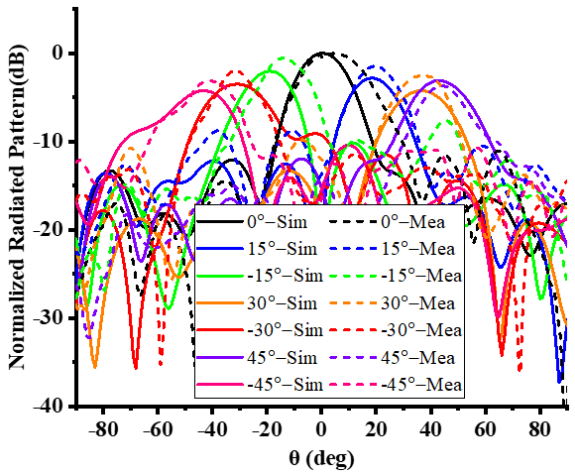

(a)

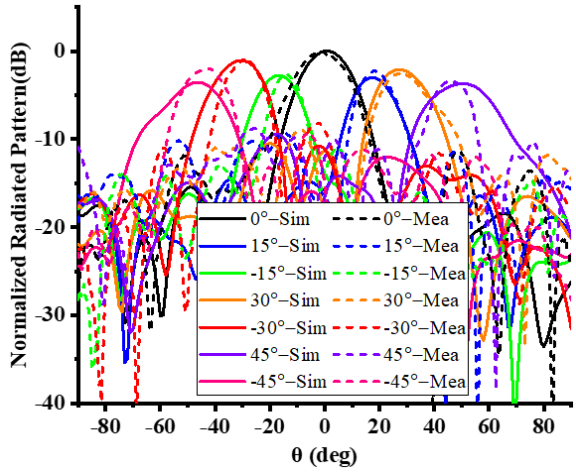

(b)

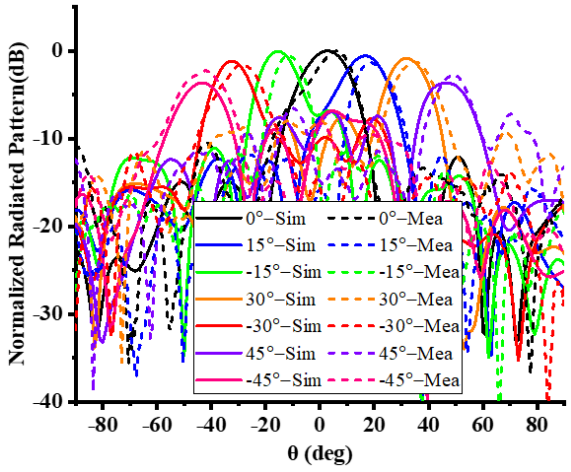

(c)

Fig. 17. Measured and simulated patterns at (a) 4, (b) 5, and (c) 6 GHz.

between adjacent elements becomes shorter. At 4 GHz, the coupling becomes so strong that the reflection phase of the certain element is determined not only by the RF switch state on itself but also by those on the elements near it. As the element is affected by its two adjacent elements along the y-axis the most, the number of the states for a certain element changes from 2 to 2^3, which is shown in Fig. 13. The reflection phase of these eight states at 4 GHz is given in Table V. It can be seen that the reflection phase of the unit cell is related to the number of "0" in the states. When there are three "0" in the states, the reflection phase is about −105°. With two "0," it is about 109°. With one "0," it is about 85°. And with no "0," it is about 77°.

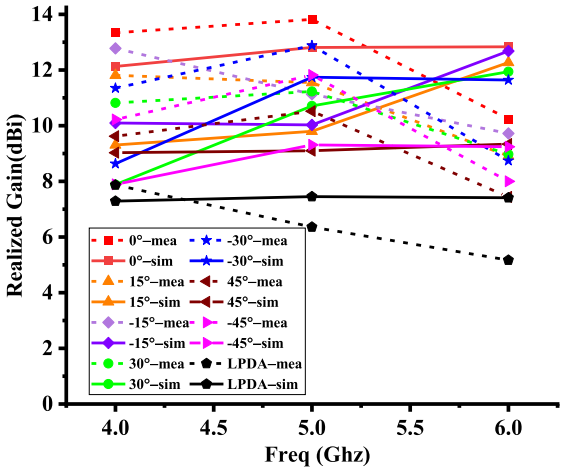

Fig. 18. Measured and simulated gains.

TABLE VI
MAX APERTURE EFFICIENCY OF THE REFLECTARRAY

Freq (GHz)	4	5	6
Measurement	25.85%	18.48%	5.63%
Simulation	19.56%	14.66%	10.26%

In this work, only three elements along the y-axis are considered. For the elements with stronger coupling, more elements should be considered, and elements along the x-axis may also need to be considered. This way of calculating the reflection phase is called the strong coupling elements reflection phase calculation (SCERPC) method.

Then, the SCERPC at 4 GHz is applied in the PSO, and the radiation patterns are calculated. Simulated and calculated radiation patterns from PSO with SCERPC at 4 GHz are shown in Fig. 14. It can be seen that the simulated radiation patterns agree well with the calculated results. The simulated SLLs are mostly below -10 dB, approximately worse than the calculated ones by about 5 dB.

IV. SIMULATED AND MEASURED RESULTS OF THE PROPOSED REFLECTARRAY

To validate the performance of the proposed beam-scanning wideband reflectarray, a prototype is fabricated, simulated, and measured. The photograph of the prototype is shown in Fig. 15. The reflectarray is connected to a microcontroller to control the states of the RF switches on the reflecting surface.

The reflection coefficient of the feed antenna is shown in Fig. 16. The simulated and measured results agree well. The reflection coefficient is mostly below -10 dB from 2.6 to 7 GHz.

Fig. 17 presents the measured and simulated radiation patterns. The measured and simulated radiation patterns are in good agreement. When the beam scans from $-45°$ to 45°, the radiation patterns remain stable. In most cases, the SLL is below -8 dB.

Fig. 18 shows the measured and simulated gains of the reflectarray and the feed antenna. It can be seen that the gain is between 7.89 and 13.82 dBi, with the beam scanning ranging from $-45°$ to 45°. The gain of the LPDA is approximately 7 dBi. Table VI shows the max aperture efficiency of the reflectarray, with the beam direction varying. There are some differences between the measured results and the simulated results in terms of beam direction and the gain, which may be attributed to the fabrication and measurement errors.

TABLE VII
COMPARISON WITH REPORTED RECONFIGURABLE REFLECTARRAYS

Ref. No.	Bandwidth	Phase bits	Scan range	Tuning devices	Device number in one element	Profile(λ)	Max Aperture Eff. [%]
[6]	10%	1	±45°	Pin diode	2	0.07	26
[7]	22%	2	±60°	Pin diode	8	0.07	35
[11]	7.4%	1	±60°	Pin diode	2	0.08	20
[13]	32%	1	±60°	Pin diode	4	0.12	24
[17]	15%	1	±50°	Pin diode	1	0.11	28.5
This work	40%	1	±45°	RF switch	1	0.3	25.8

The proposed design and some recent related works are compared in Table VII. Although the profile of the proposed beam-scanning reflectarray is relatively high, it realizes the widest bandwidth. Additionally, using RF switches as tuning devices reduces the structural complexity of the element.

V. CONCLUSION

A beam-scanning reflectarray based on tightly coupled 1-bit reconfigurable unit cells is proposed. By loading RF switches on the delay lines of the unit cells, the reflection phase can be switched. This method reduces the structural complexity of the elements compared with those loaded by p-i-n diodes. Additionally, PSO is introduced to optimize the switch states on the reflecting surface, significantly improving the SLLs of the radiation pattern. Finally, a novel method of calculating the reflection phase of strongly coupled unit cells is proposed. The proposed design can achieve ±45° beam scanning from 4 to 6 GHz.

REFERENCES

[1] S. Gao, Y. J. Guo, S. A. Safavi-Naeini, W. Hong, and X. Yang, "Guest editorial low-cost wide-angle beam-scanning antennas," *IEEE Trans. Antennas Propag.*, vol. 70, no. 9, pp. 7378–7383, Sep. 2022.

[2] S. V. Hum, M. Okoniewski, and R. J. Davies, "Realizing an electronically tunable reflectarray using varactor diode-tuned elements," *IEEE Microw. Wireless Compon. Lett.*, vol. 15, no. 6, pp. 422–424, Jun. 2005.

[3] M. E. Trampler and X. Gong, "Phase-agile dual-resonance single linearly polarized antenna element for reconfigurable reflectarray applications," *IEEE Trans. Antennas Propag.*, vol. 67, no. 6, pp. 3752–3761, Jun. 2019.

[4] M. Riel and J.-J. Laurin, "Design of an electronically beam scanning reflectarray using aperture-coupled elements," *IEEE Trans. Antennas Propag.*, vol. 55, no. 5, pp. 1260–1266, May 2007.

[5] H. Yang, F. Yang, S. Xu, M. Li, X. Cao, and J. Gao, "A 1-bit multipolarization reflectarray element for reconfigurable large-aperture antennas," *IEEE Antennas Wireless Propag. Lett.*, vol. 16, pp. 581–584, 2017.

[6] J. Hu, P.-L. Chi, and T. Yang, "Novel 1-bit beam-scanning reflectarray with switchable linear, left-handed, or right-handed circular polarization," *IEEE Trans. Antennas Propag.*, vol. 71, no. 2, pp. 1548–1556, Feb. 2023.

[7] F. Wu et al., "A 2-bit circularly-polarized reconfigurable reflectarray using PIN-diode-tuned crossed-bowtie patch elements," *IEEE Trans. Antennas Propag.*, vol. 71, no. 9, pp. 7299–7309, Sep. 2023.

[8] G. Perez-Palomino et al., "Accurate and efficient modeling to calculate the voltage dependence of liquid crystal-based reflectarray cells," *IEEE Trans. Antennas Propag.*, vol. 62, no. 5, pp. 2659–2668, May 2014.

[9] L. Cai, Z. H. Jiang, and W. Hong, "Evaluation of reconfigurable reflectarray antenna element at 19 GHz based on highly anisotropic liquid crystal material," in *Proc. IEEE Int. Conf. Comput. Electromagn. (ICCEM)*, Shanghai, China, Mar. 2019, pp. 1–3.

[10] Y. Zhang, S. Tang, J. Rao, C.-Y. Chiu, X. Chen, and R. Murch, "A dual-port dual-beam pattern-reconfigurable antenna with independent 2-D beam-scanning," *IEEE Trans. Antennas Propag.*, vol. 72, no. 10, pp. 7628–7643, Oct. 2024.

[11] F. Wu, R. Lu, J. Wang, Z. H. Jiang, W. Hong, and K.-M. Luk, "A circularly polarized 1 bit electronically reconfigurable reflectarray based on electromagnetic element rotation," *IEEE Trans. Antennas Propag.*, vol. 69, no. 9, pp. 5585–5595, Sep. 2021.

[12] M. Zhang et al., "Design of novel reconfigurable reflectarrays with single-bit phase resolution for Ku-band satellite antenna applications," *IEEE Trans. Antennas Propag.*, vol. 64, no. 5, pp. 1634–1641, May 2016.

[13] F. Wu, R. Lu, J. Wang, Z. H. Jiang, W. Hong, and K.-M. Luk, "Circularly polarized one-bit reconfigurable ME-dipole reflectarray at X-band," *IEEE Antennas Wireless Propag. Lett.*, vol. 21, no. 3, pp. 496–500, Mar. 2022.

[14] W. Xue, J. Han, C. Qiao, and L. Li, "Design of 1-bit digital coding reconfigurable reflectarray using aperture-coupled elements controlled by PIN diodes," in *Proc. Int. Conf. Microw. Millim. Wave Technol. (ICMMT)*, Chengdu, China, May 2018, pp. 1–3.

[15] Z. Wang et al., "1 bit electronically reconfigurable folded reflectarray antenna based on p-i-n diodes for wide-angle beam-scanning applications," *IEEE Trans. Antennas Propag.*, vol. 68, no. 9, pp. 6806–6810, Sep. 2020.

[16] E. Carrasco, M. Barba, and J. A. Encinar, "X-band reflectarray antenna with switching-beam using PIN diodes and gathered elements," *IEEE Trans. Antennas Propag.*, vol. 60, no. 12, pp. 5700–5708, Dec. 2012.

[17] Y. Hao, C. Deng, X. Cao, Y. Yin, and K. Sarabandi, "A high aperture efficiency 1-bit reconfigurable reflectarray antenna with extremely low power consumption," *IEEE Trans. Antennas Propag.*, vol. 72, no. 1, pp. 1015–1020, Jan. 2024.

[18] T. Yin, J. Ren, Y. Chen, K. Xu, and Y. Yin, "Highly integrated reconfigurable shared-aperture EM surface with multifunctionality in transmission, reflection, and absorption," *IEEE Trans. Antennas Propag.*, vol. 72, no. 8, pp. 6789–6794, Aug. 2024.

[19] W. Wu, K.-D. Xu, Q. Chen, T. Tanaka, M. Kozai, and H. Minami, "A wideband reflectarray based on single-layer magneto-electric dipole elements with 1-bit switching mode," *IEEE Trans. Antennas Propag.*, vol. 70, no. 12, pp. 12346–12351, Dec. 2022.

[20] H. Luyen, Z. Yang, M. Gao, J. H. Booske, and N. Behdad, "A wideband, single-layer reflectarray exploiting a polarization rotating unit cell," *IEEE Trans. Antennas Propag.*, vol. 67, no. 2, pp. 872–883, Feb. 2019.

[21] W. Li, S. Gao, L. Zhang, Q. Luo, and Y. Cai, "An ultra-wide-band tightly coupled dipole reflectarray antenna," *IEEE Trans. Antennas Propag.*, vol. 66, no. 2, pp. 533–540, Feb. 2018.

[22] W. Li, H. Tu, Y. He, L. Zhang, S.-W. Wong, and S. Gao, "A novel wideband tightly coupled dual-polarized reflectarray antenna," *IEEE Trans. Antennas Propag.*, vol. 71, no. 6, pp. 5422–5427, Jun. 2023.

[23] Z. Ai, W. Li, Y. He, and L. Z. S.-W. Wong, "Design of the one-bit unit cell for a broadband reflectarray," in *Proc. IEEE Int. Workshop Radio Freq. Antenna Technol. (iWRF&AT)*, Shenzhen, China, May 2024, pp. 332–334.

[24] Y. Cai et al., "A novel ultrawideband transmitarray design using tightly coupled dipole elements," *IEEE Trans. Antennas Propag.*, vol. 67, no. 1, pp. 242–250, Jan. 2019.

[25] P. Nayeri, F. Yang, and A. Z. Elsherbeni, "Design and experiment of a single-feed quad-beam reflectarray antenna," *IEEE Trans. Antennas Propag.*, vol. 60, no. 2, pp. 1166–1171, Feb. 2012.

Wenting Li (Member, IEEE) received the B.S. degree in electronic information engineering and the M.S. degree in electromagnetic field and microwave technology from Northwestern Polytechnical University, Xi'an, China, in 2011 and 2014, respectively, and the Ph.D. degree in electronic engineering from the University of Kent, Canterbury, U.K., in 2019.

He is currently an Assistant Professor with the College of Electronics and Information Engineering, Shenzhen University, Shenzhen, China. His current research interests include reflectarray antennas, reconfigurable antennas, circularly polarized antennas, and multibeam antennas.

Dr. Li was a recipient of Shenzhen Overseas High-Caliber Personnel Level C ("Peacock Plan Award" C).

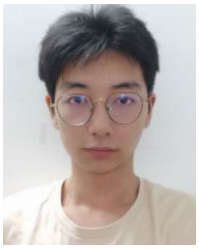

Zhikang Ai was born in Hubei, China, in 2000. He received the B.S. degree in communication engineering from Nanchang University, Nanchang, China, in 2022. He is currently pursuing the M.S. degree in communication engineering with Shenzhen University, Shenzhen, China.

His current research interests include wideband beam-scanning reflectarrays and tightly coupled array antennas.

Yejun He (Senior Member, IEEE) received the Ph.D. degree in information and communication engineering from the Huazhong University of Science and Technology (HUST), Wuhan, China, in 2005.

From 2005 to 2006, he was a Research Associate with the Department of Electronic and Information Engineering, The Hong Kong Polytechnic University, Hong Kong. From 2006 to 2007, he was a Research Associate with the Department of Electronic Engineering, Faculty of Engineering, The Chinese University of Hong Kong, Hong Kong. In 2012, he joined the Department of Electrical and Computer Engineering, University of Waterloo, Waterloo, ON, Canada, as a Visiting Professor. From 2013 to 2015, he was an Advanced Visiting Scholar (Visiting Professor) with the School of Electrical and Computer Engineering, Georgia Institute of Technology, Atlanta, GA, USA. From 2023 to 2024, he was an Advanced Research Scholar (Visiting Professor) with the Department of Electrical and Computer Engineering, National University of Singapore, Singapore. He has been a Faculty Member with Shenzhen University, Shenzhen, China, where he is currently a Full Professor with the College of Electronics and Information Engineering. His research interests include wireless communications, antennas, and radio frequency (RF).

Dr. He was a recipient of Shenzhen Overseas High-Caliber Personnel Level B (Peacock Plan Award B) and Shenzhen High-Level Professional Talent (Local Leading Talent), Second Prize of Guangdong Provincial Science and Technology Progress Award in 2023, the 10th Guangdong Provincial Patent Excellence Award in 2023, the Second Prize of Shenzhen Science and Technology Progress Award in 2017, the Three Prize of Guangdong Provincial Science and Technology Progress Award in 2018, and the 2022 IEEE APS Outstanding Chapter Award. He is also an Associate Editor for IEEE TRANSACTIONS ON ANTENNAS AND PROPAGATION, IEEE TRANSACTIONS ON VEHICULAR TECHNOLOGY, IEEE TRANSACTIONS ON MOBILE COMPUTING, *IEEE Antennas and Propagation Magazine*, IEEE ANTENNAS AND WIRELESS PROPAGATION LETTERS, and *International Journal of Communication Systems*, *China Communications*, and *ZTE Communications*.

Chong Zhang (Member, IEEE) received the B.S. degree in electronic information engineering and the M.S. and Ph.D. degrees in electromagnetic field and microwave technology from Northwestern Polytechnical University, Xi'an, China, in 2008, 2011, and 2016, respectively.

He is currently an Assistant Professor with the School of Information Science and Engineering, Shenyang University of Technology, Shenyang, China. His current research interests include reflectarray antennas, circularly polarized antennas, and 3-D-printed antennas.

Yao Gao received the M.S. degree in electromagnetic field and microwave technology from Northwestern Polytechnical University, Xi'an, China, in 2012, and the Ph.D. degree in physics from Université Pierre et Marie Curie, Paris, France, in 2016.

He is currently with the College of Information Engineering, Chang'an University, Xi'an. His current research interests include circularly polarized antennas, microwave devices, and ground-penetrating radar (GPR).

Ruiyang Li received the B.E. degree in electronics and information engineering and the Ph.D. degree in electronic science and technology from Northwestern Polytechnical University, Xi'an, China, in 2012 and 2018, respectively.

From 2014 to 2016, she was a Visiting Research Student with the University of Ottawa, Ottawa, ON, Canada. She is currently a Lecturer of electrical engineering with the School of Information Engineering, Zhengzhou University, Zhengzhou, China. Her research interests include unidirectional electrically small antennas, characteristic modes, and antenna shape synthesis.

Dr. Li received the Honorable Mention Award of the 2017 IEEE Asia–Pacific Conference on Antennas and Propagation.

Steven Gao (Fellow, IEEE) received the Ph.D. degree in microwave engineering from Shanghai University, Shanghai, China, in 1999.

He was a Post-Doctoral Research Fellow with the National University of Singapore, Singapore, a Research Fellow with Birmingham University, Birmingham, U.K., a Visiting Research Scientist at the Swiss Federal Institute of Technology, Zürich, Switzerland, a Visiting Fellow at Chiba University, Chiba, Japan, a Visiting Scientist at the University of California, Santa Barbara, CA, USA, a Senior Lecturer, Reader, and the Head of an Antenna and Microwave Group, Northumbria University, Newcastle upon Tyne, U.K., and the Head of the Satellite Antennas and RF System Group, with Surrey Space Centre, University of Surrey, Surrey, U.K. He is currently a Professor and the Chair of RF and Microwave Engineering with the University of Kent, Canterbury, U.K. Since 1994, he has been with China Research Institute of Radiowave Propagation, Xinjiang, China. He has been a Professor with the University of Kent, since 2013. He has co-authored *Circularly Polarized Antennas* (IEEE-Wiley, 2014), over 250 papers and several patents. His current research interests include smart antennas, phased arrays, MIMO, satellite antennas, microwave/mm-wave/THz circuits, satellite and mobile communications, and radar (UWB radar and synthetic-aperture radar) and wireless power transfer.

Dr. Gao is a Fellow of IET, U.K. He was a Coeditor of the Space Antenna Handbook (Wiley, 2012). He was a General Chair of LAPC 2013 and an Invited or Keynote Speaker at some international conferences such as the AES'2014, the IWAT'2014, the SOMIRES'2013, and the APCAP'2014. He is an IEEE AP-S Distinguished Lecturer. He is an Associate Editor of IEEE TRANSACTIONS ON ANTENNAS AND PROPAGATION, *Radio Science*, and an Editor-in-Chief of the Wiley Book Series on *Microwave and Wireless Technologies*.